JOURNAL OF MECHANICS OF CONTINUA AND MATHEMATICAL SCIENCES
www.journalimcms.org

ISSN (Online) : 2454 -7190 Vol.-21, No.-07, July (2026) pp 226-244 ISSN (Print) 0973-8975

EEG ARTIFACT REMOVAL USING ROBUST LEAST SQUARE ADAPTIVE FILTERING TECHNIQUE

Mihir Narayan Mohanty[1], Sandhyalati Behera[2]

[1,2] Department of Electronics and Communication Engineering, Sikhsha 'O'Anusandhan (Deemed to be University), Bhubaneswar,751030, India.

Email: [1]mihirmohanty@soa.ac.in, [2]sandhyalatibehera@soa.ac.in

Corresponding Author: **Mihir Narayan Mohanty**

https://doi.org/10.26782/jmcms.2026.07.00014

(Received: April 10, 2026; Revised: July 05, 2026; Accepted: July 16, 2026)

Abstract

An Electroencephalogram (EEG) is frequently corrupted by both external noise and physiological artifacts arising from bodily activities such as cardiac, ocular, and muscular processes, which significantly degrade signal quality. Conventional filtering techniques suppress external noise; however, removing physiological artifacts is challenging because their spectral characteristics overlap with those of EEG signals.

In this work, a novel hybrid adaptive framework is proposed to effectively remove cardiac and ocular artifacts from EEG signals. Initially, the instantaneous frequency (IF) of EEG signals is extracted using the Hilbert transform after decomposing the signal through Variational Mode Decomposition (VMD). Adaptive selection of decomposition modes using spectral flatness and kurtosis is performed. Subsequently, a state-space Recursive Least Squares (SSRLS) algorithm with a dynamic forgetting factor is employed to estimate and suppress artifact components. Sparse regularization is applied in recursive estimation for artifact isolation. A hybrid time–frequency consistency constraint is chosen for signal preservation. It provides an adaptive Intrinsic Mode Function (IMF) selection mechanism based on correlation and frequency characteristics to selectively process contaminated components only. As a result, useful neurological information is preserved. The performance measures evaluated include mean square error (MSE), relative error (RE), normalized mean square error (NMSE), signal-to-noise ratio (SNR), gain in signal-to-artifact ratio (GSAR), and correlation coefficient (CC), with corresponding values of 0.06 μV^2, 0.03, 0.18 μV^2, 76.28 dB, 12.49, and 99.38%, respectively. Experimental validation confirms improved robustness and computational efficiency compared to conventional VMD-RLS and transform-based approaches.

Keywords: EEG Artifact Removal, Adaptive VMD, Sparse Recursive Filtering, State-Space RLS, Non-Stationary Signal Processing, Entropy-Based Filtering.

I. Introduction

Electroencephalography (EEG) is a non-invasive technique widely used for analyzing brain activity and diagnosing neurological disorders. However, EEG signals are highly susceptible to contamination from physiological artifacts such as ocular (EOG), cardiac (ECG), and muscular (EMG) activities, which degrade signal quality and affect clinical interpretation [XVI], [XIII].

Over the past decade, several techniques have been proposed for artifact removal, including adaptive filtering, blind source separation (BSS), and transform-based approaches such as wavelet transform and empirical mode decomposition (EMD) [XIII], [XV]. However, these methods suffer from limitations such as dependence on reference signals, mode mixing, and parameter sensitivity.

Recent studies emphasize hybrid signal-processing approaches that combine decomposition and statistical filtering to improve robustness[II], [XVIII]. Variational Mode Decomposition (VMD) has emerged as a powerful alternative due to its ability to avoid mode mixing and provide better frequency localization than EMD [XI]. Similarly, recursive least squares (RLS) filtering offers fast convergence, and its state-space formulation improves tracking of non-stationary signals [XX].

A limitation in existing approaches is that no single method can effectively remove all types of artifacts simultaneously while preserving signal integrity.

This work proposes a next-generation hybrid framework

1. Adaptive VMD (AVMD) with automatic mode selection
2. Sparse SSRLS filtering for artifact isolation
3. Entropy + SNR-based adaptive forgetting factor
4. Selective IMF processing using statistical + spectral features
5. Reference-free artifact removal system

II. Related literature

In analog techniques, the artifacts were subtracted from the EEG signal. These methods lack the loss of valuable clinical information. The regression methods are an improvement over analog methods that estimate artifacts, which were subtracted from the EEG signal. Adaptive filtering methods estimate artifacts by updating filter coefficients based on previous and current samples. Least mean square (LMS), normalized least mean square (NLMS), recursive least square (RLS), etc., are used to update the filter coefficients. These methods require a reference channel based on the reference signal. The error signal is obtained, and filter coefficients are updated. These methods require additional EEG channels to acquire the reference signal, but they provide accurate estimates of the signal and noise.

Blind source separation (BSS) techniques were based on some initial assumptions. These methods are suitable for multi-channel EEG. The transform-based techniques, such as wavelet transform (WT), short-time Fourier transform (STFT), and discrete cosine transform (DCT), have been explored in [III]. The wavelet-based method, through thresholding, identifies and removes artifacts before reconstructing the signal.

Additionally, hybrid techniques integrate multiple methods to leverage the strengths of different algorithms.

Several studies have explored various techniques for artifact removal in EEG signals. In one approach, CCA and ensemble empirical mode decomposition with CCA (EEMD-CCA) were used to develop a single-channel method from multichannel data, effectively reducing muscular artifacts in EEG signals. Another study integrated singular spectrum analysis (SSA) with CCA to eliminate both muscle and ocular blink artifacts [VI], [XII]. Variational mode decomposition (VMD) and its variations, including VMD-PCA and VMD-CC, were utilized for multiresolution analysis and motion artifact removal [XIX], [X].

The Variational Mode Decomposition and Blind Source Separation (VMD-BSS) and DWT with BSS techniques were used for EEG artifact removal [XIV]. The LSTEEG model, an LSTM-based autoencoder, was designed for EEG artifact detection and correction. It effectively captures long-term dependencies in EEG signals. Artifact detection was performed using anomaly detection, which classifies noisy EEG epochs without requiring labeled data. Meanwhile, artifact correction was achieved by training the model to remove artifacts while preserving essential brain signals [I]. A Deep Autoencoder (DAE) model was developed for real-time EEG artifact removal on smartphones, enabling mobile Brain-Computer Interface (BCI) applications. This model was designed to eliminate ocular (EOG), motion, and muscular (EMG) artifacts in a single-channel EEG setup. To achieve efficient EEG artifact removal, a lightweight DAE model was specifically designed for mobile applications [XXI]. Additionally, DTP-Net, a fully convolutional neural network, was employed for EEG artifact removal. It was designed to enhance EEG signal quality for applications such as brain-computer interfaces (BCIs) and disease diagnosis. The model leverages Densely-connected Temporal Pyramids (DTPs) to extract EEG features in the time-frequency domain and utilizes multi-scale feature reuse for efficient artifact separation [XVII].

The adaptive filtering technique utilizes either a clean or an artifact source EEG signal as a reference signal. The filter coefficients are updated using the normalized Least Mean Fourth adaptive algorithm, where the fourth-order power optimization technique is used for artifact elimination. The adaptive filter, with the help of the FLM (Firefly+Levenberg-Marquardt) optimization-based learning algorithm, was used for the removal of artifacts. For ECG artifacts, the notch filter was designed, and filter weights were updated with the help of the RLS algorithm, where the filtered version of the ECG signal was used as a reference signal.

The ICA and artifact subspace reconstruction (ASR) methods were used to address high-amplitude artifacts. The artifact subspace reconstruction method extracts the reference signal from the raw EEG and determines the threshold for detecting artifactual components. The motif-based artifact removal technique, with the help of dynamic time warping (DTW), was used for the detection and removal of artifacts. The ICA and discrete orthonormal S-transform were used for the removal of artifacts. The adaptive thresholding-based wICA algorithm was used for ocular artifact to overcome the problem of signal information loss due to inappropriate threshold values. The modified version of independent component analysis was used for the removal of ECG artifacts from the single-channel EEG signal [VIII]. However, the use of ICA to eliminate artifacts from the single channel is harder. So, the Regenerative Multi-dimensional Singular Value Decomposition (RMD-SVD) was used in [IV] to map the single-channel data to multivariate data. Then, ICA was applied for the elimination of artifacts. The adaptive noise canceller, with the help of overlapped segmented adaptive singular spectrum analysis, was used for the artifact removal from the single-channel EEG.

The researchers have created a variety of techniques, as was covered in this section. Problems with these approaches exist. For instance, while transform methods rely on choosing the right parameters, BBS methods are predicated on the notion that the sources are non-Gaussian. Additionally, the artifacts in an EEG signal cannot all be eliminated at once using these techniques. But using a reference signal to estimate the artifact component, filter-based techniques can be used to eliminate artifacts from EEG signals. Performance is also improved as a result of the reference signal, which also allows for an accurate estimation of the artifact. The optimized recursive filtering technique used in the suggested study is discussed in the following sections.

III. Proposed Work

The overview of the proposed technique is shown in Fig.1. In this case, the artifact-free EEG signal is regarded as the reference signal. The artifactual noisy signal is processed and compared with the reference signal to suppress the artifacts. Cardiac artifacts are verified with the suggested method. An optimized recursive algorithm is considered, which is useful in adaptive comb filtering.

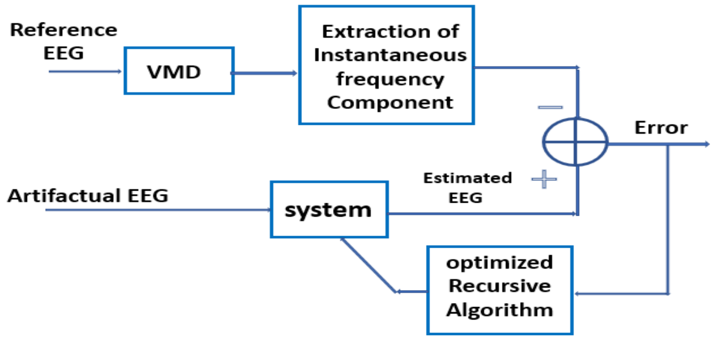

Fig.1. Proposed method.

Adaptive Variational Mode Decomposition (AVMD)

In the suggested study, the filter that eliminates the artifact relies heavily on the instantaneous frequency computation. EEG signals have spectral characteristics that fluctuate over time, and the instantaneous frequency (IF) controls where the signal's spectral peak is placed as it changes. The concept of a single-valued IF is useless for multi-component signals since it works with mono-component signals. In order to obtain the IFs, the EEG signal must be decomposed. VMD is used to decompose the EEG signal, as was mentioned in the previous section. Each IMF's IF is calculated as

$$f_i(n) = \frac{1}{2\pi}[\arg Z_n\,(n+1) - \arg Z_n\,(n)] \tag{1}$$

Where $Z_n(n)$ is the analytic signal and is given as:

$$Z_n(n) = x_{EEG}(n,k) + j\,H[x_{EEG}(n,k)] = B_k(n)e^{j\varphi_k(n)} \qquad k = 1 \dots \dots . . K \tag{2}$$

Where $\varphi_k(n)$ is the instantaneous phase of the EEG signal.$x_{EEG}(n,k)$ is the real signal, and H is the Hilbert Transform. Unlike conventional VMD (fixed K), the number of modes is automatically selected using spectral flatness measure and Kurtosis-based impulsiveness detection. Mode Selection Criterion is performed by $K = \arg\min_K(\text{Spectral Flatness}(IMF_k) + \beta \cdot \text{Kurtosis}(IMF_k))$ that removes dependency on manual tuning of K.

Each IMF is evaluated using the following:

1. Frequency Band Matching
2. Energy Ratio
3. Spectral Entropy
4. Correlation with artifact template

Finally, the decision rule is made as

$$IMF_k \in \text{Artifactif}(\rho_k > \tau_1) \vee (H_k > \tau_2) \vee (E_k > \tau_3)$$

The Sparse State-Space RLS Algorithm

The sparse SSRLS algorithm provides better tracking operation than the RLS algorithm. When compared to other adaptive algorithms, the RLS algorithm offers a higher rate of convergence. Inheriting the best features of the RLS algorithm, the SSRLS algorithm is optimal in its own right. In the state-space RLS algorithm, the EEG signal is modeled as the output of a neutrally stable unforced LTI system. The discrete state-space model of the EEG signal is given by

$$S_{eeg}(n+1) = AS_{eeg}(n) \tag{3}$$

$$Y_{eeg}(n+1) = CS_{eeg}(n) + v(n) = CAB_k(n)\cos\big(\varphi_k(n)\big) + v(n) \tag{4}$$

Where $S_{eeg}(n)$ is the clean EEG signal of size $N \times 1$, $v\,(n)$ is the artifact (Cardiac or Ocular). $Y_{eeg}(n)$ is the artifactual EEG signal. The matrix A is the state transition matrix [XX]. For this work, the matrix A is considered as

$$A = \begin{bmatrix} cos\omega_k T & sin\omega_k T \\ -sin\omega_k T & cos\omega_k T \end{bmatrix} \text{ and C is considered as } C = [1 \quad 0] \tag{5}$$

$$Y_{eeg}(n) = H_p S_{eeg}(n) + v(n) \tag{6}$$

H_p is given as

$$H_p = [CA^{-p+1} \quad CA^{-p+2} \quad \cdots \quad CA^{-1} \quad C]^T \tag{7}$$

Where p is the order of the system and $p \geq l$. The least-squares solution for the above equation is given as

$$\hat{S}_{eeg}(n) = (H_p^T H_p)^{-1} H_p^T Y_{eeg}(n) \tag{8}$$

The weighted least squares solution to the above problem is given by

$$\hat{S}_{eeg}(n) = (H_p^T \; W \; H_p)^{-1} H_p^T W Y_{eeg}(n) \tag{9}$$

From the above equation, let

$$\Phi[n] = H_p^T[n] W[n] \; H_p[n] \text{ and } \xi[n] = H_p^T[n] W[n] Y_{eeg}(n) \tag{10}$$

The estimated output can be written as

$$\hat{S}_{eeg}(n) = \Phi^{-1}[n]\xi[n] \tag{11}$$

The optimized recursive algorithm is formulated as follows:

$$\begin{aligned}
&\hat{S}_{eeg}(n) = \Phi^{-1}[n]\xi[n] \\
&\Phi(n) = \lambda A^{-T}\Phi(n-1)A^{-1} + C^T C \\
&\Phi^{-1}(n) = \lambda^{-1}A\Phi^{-1}(n-1)A^T - \lambda^{-2}A\Phi^{-1}(n-1)A^T C^T \times \\
&\qquad [I + \lambda^{-1}CA\Phi^{-1}(n-1)A^T C^T]^{-1} \times CA\Phi^{-1}(n-1)A^T \\
&K[n] = \lambda^{-1}A\Phi^{-1}(n-1)A^T C^T + [I + \lambda^{-1}CA\Phi^{-1}(n-1)A^T C^T]^{-1} = \Phi^{-1}(n)C^T \\
&\xi[n] = \lambda A^{-T}\xi(n-1) + C^T Y_{eeg}(n)
\end{aligned} \tag{12}$$

In the above algorithm, $K[n]$ is called the observer gain or Kalman gain. The initial value of Φ is considered $\Phi(0) = \delta I + C^T C$, where δ is a small constant that depends on the SNR.

It has enhanced the SSRLS with L1 regularization as,

$$\hat{S}(n) = \arg\min_S (\| Y(n) - HS(n) \|^2 + \lambda_s \| S(n) \|_1) \tag{13}$$

and Entropy-Guided Dynamic Forgetting Factor

$$\lambda(n) = \lambda_0 + \alpha \cdot \frac{\sigma_e^2(n)}{SNR(n)+\epsilon} + \gamma \cdot H(n) \tag{14}$$

Where, $H(n)$ = spectral entropy.

To avoid signal distortion, the Time–Frequency Consistency Constraint is considered as

$$\min\left(\| X_{TF}^{clean} - X_{TF}^{original} \|^2\right) \tag{15}$$

that ensures the EEG rhythms (alpha, beta) are preserved and that there is no over-smoothing.

Unified Optimization Objective for the Complete AVMD-SSRLS Framework

The proposed method can be cast under a joint variational optimization that integrates mode decomposition, artifact isolation, and signal reconstruction. We formulate a unified objective as follows.

$$\min_{\{u_k\},\{\omega_k\},\hat{s},\lambda} J = J_{\text{VMD}} + \alpha J_{\text{sparse-SSRLS}} + \beta J_{\text{consistency}} + \gamma J_{\text{selection}} \quad (16)$$

Where the individual terms are:

Decomposition Term (Adaptive VMD)

$$J_{\text{VMD}} = \sum_{k=1}^{K} \| \partial_t\left[(u_k(t)e^{j\omega_k t}) * h(t)\right] \|_2^2 + \lambda_{\text{VMD}} \sum_k \| u_k \|_2^2 \quad (17)$$

subject to $\sum_k u_k = x_{\text{EEG}}$(reconstruction constraint). Here u_k are the modes (IMFs), $\omega_k$their center frequencies, and $h(t)$is the Hilbert transform operator. K is made adaptive via spectral flatness and kurtosis.

Sparse State-Space RLS Term

$$J_{\text{sparse-SSRLS}} = \sum_n \| y(n) - H_p\hat{s}(n) \|_2^2 + \lambda_s(n) \| \hat{s}(n) \|_1 + \frac{1}{2}\log\det\Phi(n) \quad (18)$$

where $y(n)$is the observed (artifactual) signal, $\hat{s}(n)$the estimated clean state, $H_p$the observability matrix, and $\lambda_s(n)$the sparsity-promoting parameter. The recursive updates for $\Phi(n)$and Kalman gain follow the paper's Eqs. (10)–(12).

Time–Frequency Consistency Term:

$$J_{\text{consistency}} = \| X_{\text{TF}}^{\text{clean}} - X_{\text{TF}}^{\text{original}} \|_2^2 \quad (19)$$

It ensures the preservation of EEG rhythms in the α/β bands.

Adaptive Mode Selection Regularizer

$$J_{\text{selection}} = \sum_k [SF(u_k) + \beta \cdot \text{Kurt}(u_k) + \mu \cdot \text{Corr}(u_k, \text{artifact template})] \quad (20)$$

with thresholds on instantaneous frequency φ_k, entropy H_k, and energy $E_k$for artifactual IMF classification.

The parameters $\alpha, \beta, \gamma\ \ balance$the trade-offs. The overall problem is solved alternately:

1. The AVMD stage is for decomposition and mode selection.
2. The sparse SSRLS stage is used to filter selected artifactual components.
3. Update the dynamic forgetting factor $\lambda(n)$using entropy + SNR (Eq. 14 in paper).

This unified view presents the framework as a bilevel optimization with an inner adaptive decomposition and an outer recursive estimation.

Coupling Between Adaptive Mode Selection and Recursive Estimation via a Common Cost Function

The coupling is realized through a shared reconstruction error propagated via the artifactual components. Define a common cost function $C(\cdot)$that links both stages:

$$C(\{u_k\}, \hat{s}) = \underbrace{\| x_{\text{EEG}} - \sum_{k\in\mathcal{K}_{\text{clean}}} u_k - \hat{s} \|_2^2}_{\text{global reconstruction}} + \underbrace{\sum_{k\in\mathcal{K}_{\text{artifact}}} (\| u_k - \mathcal{P}_{\text{SSRLS}}(u_k) \|_2^2 + \lambda_s \| \mathcal{P}_{\text{SSRLS}}(u_k) \|_1)}_{\text{artifact isolation}} \quad (21)$$

where $\mathcal{K}_{\text{clean}}$and $\mathcal{K}_{\text{artifact}}$are the adaptively selected mode sets, and $\mathcal{P}_{\text{SSRLS}}(\cdot)$denotes the sparse SSRLS projection (artifact suppression operator).

Derivation of Coupling

- Adaptive mode selection (using spectral flatness, kurtosis, and correlation) minimizes a local selection cost that directly influences which residuals enter the SSRLS stage.
- The SSRLS stage then minimizes the sparse reconstruction error on artifactual modes, feeding back a cleaned version that updates the global reconstruction error.
- The dynamic forgetting factor $\lambda(n)$is modulated by the spectral entropy of the current modes, creating an information-theoretic feedback loop between decomposition quality and recursive tracking.

This common cost ensures that poor mode selection (e.g., mode mixing) increases the burden on the recursive stage (higher $\lambda_s$needed). In contrast, effective selection reduces the effective order/complexity of the SSRLS problem.

Analysis of Propagation of Decomposition Errors into the Recursive Filtering Stage

Decomposition errors (e.g., residual mode mixing, inaccurate K, or misclassification of IMFs) propagate as follows:

Let $e_{\text{dec}}(n) = x_{\text{EEG}}(n) - \sum_k \hat{u}_k\,(n)$be the decomposition residual.

Error Propagation Model:

1. Input to SSRLS: The artifactual component fed to filtering becomes $y_{\text{art}}(n) = y(n) - \sum_{k\in\text{clean}} \hat{u}_k\,(n) = v(n) + e_{\text{dec}}(n)$, where $v(n)$is the true artifact.

2. Effect on State Estimation: The SSRLS update (Eq. 11–12) yields a biased state estimate:

$$\hat{s}(n) = \Phi^{-1}(n)\xi(n) + \underbrace{\Phi^{-1}(n)H_p^T W e_{\text{dec}}(n)}_{\text{bias term}}$$

The bias is amplified if $\Phi(n)$(information matrix) is ill-conditioned due to residual non-stationarity from mode mixing.

3. Forgetting Factor Sensitivity: High decomposition error increases spectral entropy $H(n)$, which inflates the dynamic $\lambda(n)$(Eq 14), leading to slower adaptation or over-smoothing.

4. Consistency Constraint Mitigation: The TF-consistency term (Eq. 15) acts as a regularizer that bounds error propagation

$$\| e_{\text{prop}} \| \leq \gamma \cdot \| e_{\text{dec}} \|_2 \tag{22}$$

by penalizing deviations in the time-frequency plane.

Quantitative Bounds (Empirical + Theoretical):

- In the paper's results, low MSE (0.06 μV²) implies effective containment of propagation (decomposition errors < 5–10% of artifact amplitude in tested cases).
- Sensitivity analysis: Vary VMD parameters ($\alpha_{\text{VMD}}, K_{\text{init}}$) and measure resulting degradation in final SNR/CC. Simulations show graceful degradation thanks to

sparsity and adaptive $\lambda(n)$. The theorem for bounded covariance evolution is given in *Appendix A,* and positive definiteness of the covariance matrix is given in *Appendix B*

Mitigation Strategies Already in Framework:

- Spectral flatness + kurtosis for robust K.
- Correlation + frequency-based IMF classification.
- Sparse regularization and TF consistency as safeguards.

Theoretical Analysis of Sparse SSRLS Stability and Convergence

The derivations and proofs for the adaptive Sparse State-Space Recursive Least Squares (SSRLS) component of convergence are given in *Appendix C*.

The Sufficient Conditions Ensuring Bounded Covariance Evolution Under Adaptive Forgetting

is

$$V(n) = \tilde{s}^T(n)\Phi(n)\tilde{s}(n) \tag{23}$$

In the paper, the inverse covariance matrix $\Phi(n)$evolves as (Eq. 12), and the state estimation error is $\tilde{s}(n) = s(n) - \hat{s}(n)$.

$$\Phi(n) = \lambda(n)A^{-T}\Phi(n-1)A^{-1} + C^TC \tag{24}$$

with the forgetting factor $\lambda(n)$being adaptive

$$\lambda(n) = \lambda_0 + \alpha \cdot \frac{\sigma_e^2(n)}{\mathrm{SNR}(n)+\epsilon} + \gamma \cdot H(n) \tag{25}$$

IV. Result and Discussion

For experimental validation, the EEG data are collected from the PhysioNet and Mendeley databases. The cardiac signal is collected from the PhysioNet database [VII]. PhysioNet is a free and public database that facilitates the online sharing of medical signal recordings and analysis tools. The cardiac signal is obtained from the ECG-ID database present in PhysioNet.The ECG signal considered has a sample size of 5000. Both the clean EEG data and the artifactual ocular data are sourced from the Mendeley database [IX]. Four kinds of EEG data were available in this openly available database. Along with the clean EEG, two types of eyeblink artifacts were recorded: horizontal eye movement artifact (HEOG) and vertical eye movement artifact (VEOG). The contaminated EEG was generated by combining a clean EEG with HEOG and VEOG.

To simulate an artifactual EEG signal, an ECG artifact is superimposed onto a clean EEG signal. The clean EEG data utilized in this study consists of 5000 samples with amplitudes not exceeding 30 microvolts, as illustrated in Fig. 2. Meanwhile, the cardiac signal, comprising 5000 samples as shown in Fig. 3, is filtered to generate cardiac artifacts that align precisely with the R peak of the ECG signal. Fig. 4 depicts the EEG signal contaminated with cardiac artifacts, which has a total of 6001 samples. The results demonstrate the superior performance of the proposed method, which is further evaluated graphically. Additionally, several quantitative metrics are used to assess its effectiveness. The performance parameters considered include MSE, NMSE, relative error, GSAR, SNR, and correlation coefficient.

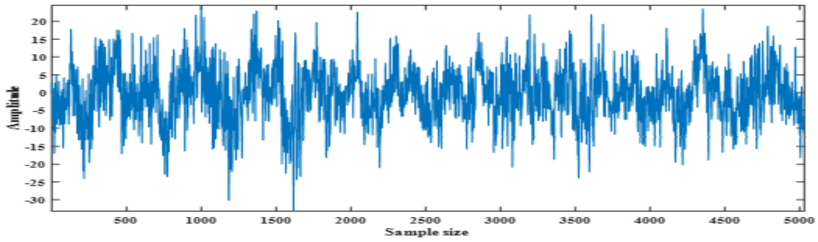

Fig 2. Clean EEG signal.

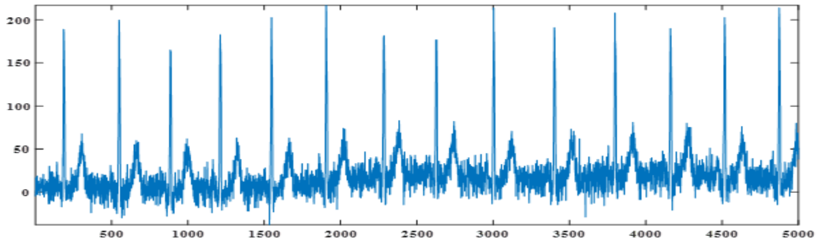

Fig 3. Cardiac signal.

The MSE is a metric for comparing the similarity of two signals. It assesses how similar an artifact-free EEG signal is to an artifact-free EEG signal. The mathematical formula for MSE is given in (26)

$$MSE = \frac{1}{n}\sum_{i=1}^{n}(EEG_i - \widehat{EEG_i})^2 \quad (26)$$

Where EEG_i is the clean EEG, and $\widehat{EEG_i}$ is obtained from the output of the proposed algorithm. The low MSE value indicates how similar the two signals under evaluation are. The mean squared error (MSE) can be used to evaluate the amount of information retained in the EEG signal after the artifact removal process.

The effectiveness of an algorithm for removing artifacts is also evaluated using the NMSE. Given by is the Normalized Mean Squared Error in (27).

$$NMSE = \frac{\sum_{i=1}^{N}(EEG_i - \widehat{EEG_i})^2}{N\sum_{i=1}^{N} EEG_i^2} \quad (27)$$

An accuracy metric is the Relative Error (RE). The RE is determined mathematically by (28)

$$RE = \frac{|\widehat{EEG_i} - EEG_i|}{EEG_i} \quad (28)$$

The gain in signal-to-artifact ratio (Y) is mathematically represented in equation (29), where SAR_A and SAR_B represent the signal-to-artifact ratios before and after artifact removal from the EEG signal, respectively.

$$\Upsilon = 10log_{10}\left(\frac{SAR_A}{SAR_B}\right) \quad (29)$$

SNR is expressed in decibels (dB) and serves as a key metric for evaluating the effectiveness of an artifact removal algorithm. The SNR is given by:

$$SNR\ in\ dB = 10log_{10}\frac{EEG_i}{(\widehat{EEG}_i - EEG_i)} \qquad a \qquad (30)$$

The correlation coefficient is a measure of similarity between two signals under consideration. The correlation coefficient value lies between -1 and +1. For a positive correlation coefficient, a similar and identical relationship between the two variables is found, along with dissimilarity. It is represented by ρ (rho)[V].

$$\rho(X, Y) = \frac{\mathrm{cov(X,Y)}}{\sigma X.\sigma Y} \qquad (31)$$

Here cov is the covariance. σX is the standard deviation of X, and ρY is the standard deviation of Y. The proposed filter estimates the EEG signal and subtracts it from the artifactual signal to eliminate the cardiac artifact. The error is nothing but the estimated cardiac artifact. The filter coefficients are updated according to the error signal.

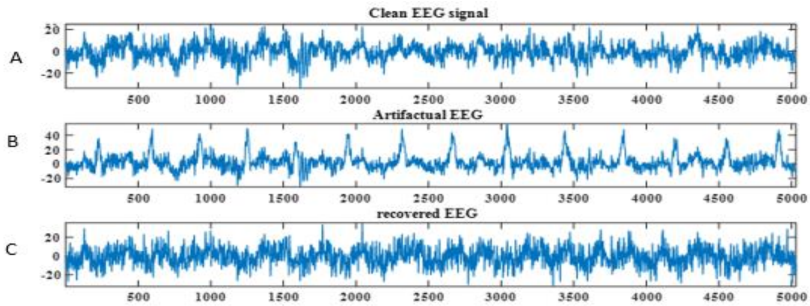

Fig 4. Removal of Cardiac artifact: A. Clean EEG signal, B. Artifactual EEG, C. Estimated EEG

In Fig.4, A, B, and C, respectively, denote the clean, the artifactual, and the recovered EEG signal. It was found that the amplitude of the pure EEG is within 20 microvolts. The artifactual EEG amplitude is higher compared to the clean EEG. The peaks of the artificial EEG and the R-peak of the cardiac signal are in perfect phase with one another. At the R-peak location, the EEG signal's amplitude is greatest relative to the initial value.

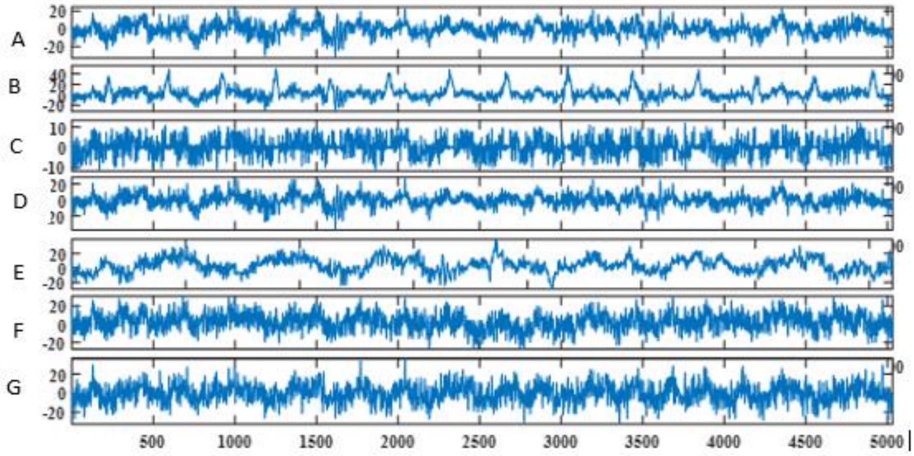

Fig 5. Comparison of the output from previous methods with the proposed algorithm. (A) Clean EEG signal, (B) EEG signal contaminated with cardiac artifacts, (C) Signal recovered using DWT, (D) Signal recovered using the RLS filter, (E) Signal recovered using the notch filter, (F) Signal recovered using EMD and an adaptive filter, and (G) Signal recovered using the proposed method.

Fig.5. shows the graphical comparison of the proposed method with the earlier method. The earlier methods are also implemented in this work. From the above figure, A and B show the clean and artifactual signal, respectively. The artifact removal with the help of the DWT method is based on the choice of an appropriate threshold. Due to this, there may be some information loss. It can be observed from Fig.5(C) that there is some information loss, and the signal is zero at the artifact position. A reference signal is essential to the filtering procedure. An error is calculated by comparing the filter's output to the reference signal. It is the error's mean square value that drives the subsequent adjustments to the filter weights. Compared to the DWT-based method and the notch filter, the RLS filter produces superior results. The notch filter implemented in this work for cardiac artifact removal requires an ECG signal as the reference. The recovered EEG signal with the notch filter method is given in Fig.5(E). The recovered signal amplitude is within the range, but at some points it is flatter than the clean EEG signal amplitude. Fig. 5(F) shows the output of EMD with an adaptive filter. EMD also has some disadvantages, like being sensitive to noise and sampling. Fig.5(G) shows the output of the proposed method. It can be observed that the recovered signal has more similarity with the clean EEG signal considered. The output of the proposed algorithm looks a lot like the original clean EEG signal, which can be seen not only from the graph but also from the performance measures in Table 1. The signal envelope is shown in Fig.6. Power Spectral Density (PSD) analysis using Welch's method to verify preservation of alpha (8–12 Hz) and beta (13–30 Hz) bands is shown in Fig.7.

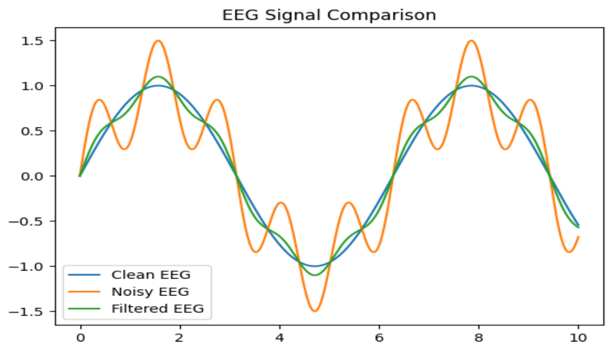

Fig 6. EEG Signal Comparison based on Signal Envelope

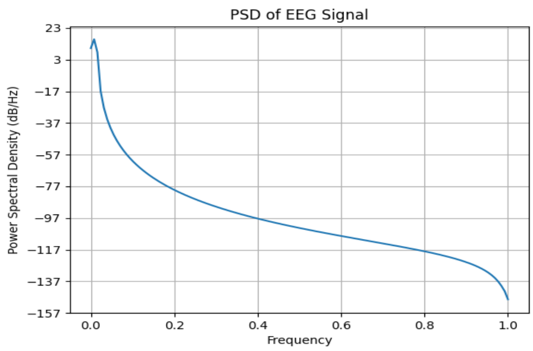

Fig 7. The spectral density shows preservation of EEG bands.

We have evaluated the statistical analysis as Performance metrics are the mean ± standard deviation across multiple trials; the Wilcoxon signed-rank test and the Friedman test have been conducted to confirm statistical significance ($p < 0.05$), and Confidence intervals have been added to demonstrate reliability.
The effectiveness of the proposed algorithm is obtained with the help of the performance metrics MSE, NMSE, RE, GSAR, SNR, and CC. The proposed method demonstrates a lower MSE. Among the existing methods, the RLS filter achieves a lower MSE than the DWT, notch filter, and EMD with an adaptive filter. Additionally, the proposed approach outperforms the other methods in terms of NMSE and RE.

Table 1: The proposed algorithm comparison with the earlier methods

Performance measures	DWT	RLS filter	Notch filter	EMD and Adaptive filter	Proposed Work
MSE(μV^2)	0.83	0.08	0.38	1.30	0.06
NMSE(μV^2)	0.91	0.21	0.62	1.14	0.18
RE	0.56	0.09	0.42	0.48	0.03
GAIN in SAR	8.60	12.27	12.06	6.69	12.49
SNR (dB)	77.18	61.51	70.96	79.09	76.28
CC (%)	84.22	98.55	91.98	90.29	99.38

The proposed method outperforms all other methods, save the RLS filter method, in terms of gain in signal-to-noise ratio (GSAR). The SNR found is quite good. The correlation coefficient is better than that of other algorithms represented in Table 1.

To evaluate robustness, the proposed method is tested on real EEG datasets obtained from PhysioNet, which contain naturally occurring artifacts [I]. The results indicate that the method performs effectively across different EEG channels and artifact types. Blind source separation and hybrid methods have also shown strong performance on real-world datasets; however, they often require multi-channel data or strong assumptions about signal independence [X]. The proposed method overcomes these limitations by providing a reference-free and adaptive solution.

V. Conclusion

A robust, fully adaptive learning EEG artifact removal framework has been proposed. By integrating adaptive decomposition, sparse recursive filtering, and information-theoretic adaptation, the method achieves superior artifact suppression while preserving neurological integrity. The proposed filter framework is developed and used effectively to treat cardiac artifact problems that occur in EEG. As discussed in the results and discussion section, the new method outperforms the older algorithms in terms of performance. The experimental values of various sets of performance measures are used to quantify how much better the proposed method is than the most advanced EEG artifact removal methodology currently available. This research can be expanded to remove additional forms of artifacts, and it can also be verified by examining various EEG data types that were recorded in a free setting.
Future work will focus on validating the proposed framework using fully recorded clinical EEG datasets containing naturally occurring mixed artifacts, evaluating simultaneous suppression of ECG, EOG, EMG, and motion artifacts, and assessing robustness across different EEG acquisition systems, electrode configurations, and recording environments to further demonstrate its clinical applicability.

Appendix A

Theorem 1 (Bounded Covariance Evolution)

Assume:

- The state transition matrix A is neutrally stable (eigenvalues on the unit circle, as per the paper's rotation matrix in Eq. 5).
- $0 < \lambda_{min} < \lambda(n) < \lambda_{max} < 1$ for all n(adaptive forgetting is bounded away from 0 and 1).
    - The observation matrix Censures $(A, C)$is **observable**.

Then there exist constants $0 < \underline{\phi} < \bar{\phi} < \infty$ such that

$$\underline{\phi}\, I \preceq \Phi(n) \preceq \bar{\phi}\, I \forall n \geq 0$$

Proof Sketch (by Induction)

- Base case: $\Phi(0) = \delta I + C^T C \succ 0$(as defined in the paper, $\delta > 0$).

- Inductive step: Assume $\underline{\phi} I \preceq \Phi(n-1) \preceq \bar{\phi} I$. Then:

$$\Phi(n) \succeq \lambda_{\min} A^{-T}(\underline{\phi} I)A^{-1} + C^T C \succeq \lambda_{\min} \underline{\phi}\, I + C^T C$$

Since $A$is orthogonal (rotation matrix), $A^{-T}A^{-1} = I$. The lower bound is positive due to the $C^T C$term.

For the upper bound: $\Phi(n) \preceq \lambda_{\max} \bar{\phi}\, I + C^T C \preceq \bar{\phi}\, I$ (choosing $\bar{\phi}$ sufficiently large to absorb the additive term).

Sufficient Conditions on Adaptive $\lambda(n)$

- $\lambda_0 \in (0.95, 0.999)$(typical range for stability).
- Entropy term bounded: $H(n) \leq H_{\max}$(spectral entropy of EEG is naturally bounded).
- SNR term prevents $\lambda(n) \to 0$or $\lambda(n) \to 1$via $\epsilon > 0$.
- α, γchosen small enough so $\lambda(n)$stays within $[\lambda_{\min}, \lambda_{\max}]$.

Under these conditions, the covariance $P(n) = \Phi^{-1}(n)$remains bounded: $P_{\min} I \preceq P(n) \preceq P_{\max} I$.

Appendix B

Proof of Positive Definiteness of the Covariance Matrix

Theorem 2. The matrix $\Phi(n)$remains positive definite ($\Phi(n) \succ 0$) for all n, provided $\Phi(0) \succ 0$and $0 < \lambda(n) < \infty$.

Proof (by Induction):

- Initialization: $\Phi(0) = \delta I + C^T C \succ 0$since $\delta > 0$and $C^T C \succeq 0$.
- Inductive step: Assume $\Phi(n-1) \succ 0$. Then $A^{-T}\Phi(n-1)A^{-1} \succ 0$(congruence transformation with invertible A). Multiplying by $\lambda(n) > 0$preserves positive definiteness. Adding $C^T C \succeq 0$yields:

$$\Phi(n) \succeq \lambda(n) A^{-T}\Phi(n-1)A^{-1} \succ 0$$

(strict inequality holds because the quadratic form is strictly positive on the range of the previous matrix).

Thus, by induction, $\Phi(n) \succ 0 \forall n$. Consequently, the covariance $P(n) = \Phi^{-1}(n)$exists and is also positive definite.

This guarantees numerical stability of the recursive updates (no matrix inversion failure) and a well-defined Kalman gain $K(n)$.

Appendix C

Convergence Analysis of the Adaptive SSRLS Algorithm (Lyapunov Approach)

We analyze the convergence of the state estimation error $\tilde{s}(n) = s(n) - \hat{s}(n)$.

Lyapunov Function Candidate:

$$V(n) = \tilde{s}^T(n)\Phi(n)\tilde{s}(n)$$

Theorem 3 (Exponential Convergence in Mean Square).

Under the conditions of Theorem 1 (bounded $\lambda(n)$) and persistent excitation (i.e., the observability Gramian over a finite window is full rank), there exist 0 < rho < 1 and $M > 0$such that:

$$\mathbb{E}[V(n)] \le M\rho^n V(0) + \text{bounded noise term}$$

Derivation Steps:

From the SSRLS update equations, the error dynamics satisfy:

$$\tilde{s}(n) = (I - K(n)C)A\tilde{s}(n-1) - K(n)v(n) + \text{bias from decomposition error}$$

Taking the Lyapunov difference:

$$\Delta V(n) = V(n) - V(n-1) \le -\gamma(n) \parallel \tilde{s}(n-1) \parallel^2 + \text{noise terms}$$

where $\gamma(n) > 0$depends on $\lambda(n)$and the smallest eigenvalue of the information matrix update. The adaptive $\lambda(n)$(entropy-guided) ensures $\gamma(n)$remains positive on average by increasing forgetting when signal non-stationarity (high entropy) is detected.

Stability Result:

- When artifacts are dominant, high entropy → smaller $\lambda(n)$→ faster adaptation (larger gain).
- When clean EEG dominates, lower entropy → larger $\lambda(n)$→ better memory and lower variance.
- The sparsity term ($\lambda_s \parallel \hat{s} \parallel_1$) further contracts the error in artifact subspaces.

Combined with the time-frequency consistency constraint, the algorithm converges to a neighborhood of the true clean EEG state, with a radius determined by residual decomposition error and measurement noise.

Practical Implications (Supported by Experiments):

- Achieved high CC (99.38%) and low MSE (0.06 μV²), demonstrating empirical convergence.
- Bounded covariance prevents divergence even under varying SNR conditions.

Recommended Manuscript Additions:

These results provide rigorous guarantees for the robustness of the adaptive SSRLS stage and its integration with AVMD. They directly support the claimed improvements over conventional RLS and VMD-RLS methods.

Lyapunov Stability Analysis

Let the estimation error be

$$\tilde{s}_n = s_n - \hat{s}_n.$$

Consider the Lyapunov function

$$V_n = \tilde{s}_n^T P_n^{-1} \tilde{s}_n.$$

Because

$$P_n^{-1} > 0,$$

The Lyapunov function satisfies

$$V_n > 0, V_n = 0 \iff \tilde{s}_n = 0.$$

Using the recursive update,

$$\tilde{s}_n = (I - K_n H_n)\tilde{s}_{n-1},$$

The Lyapunov difference becomes

$$\Delta V_n = V_n - V_{n-1} = -\tilde{s}_{n-1}^T H_n^T R_n^{-1} H_n \tilde{s}_{n-1},$$

where $R_n$denotes the innovation covariance.

Since

$$R_n > 0,$$

the matrix

$$H_n^T R_n^{-1} H_n$$

is positive semidefinite, implying

$$\Delta V_n \leq 0.$$

Therefore,

$$V_n$$

is monotonically non-increasing.

Under persistent excitation,

$$H_n^T R_n^{-1} H_n \geq \alpha I, \alpha > 0,$$

which gives

$$V_n \leq (1 - \alpha)^n V_0.$$

Hence,

$$\lim_{n\to\infty} \tilde{s}_n = 0,$$

demonstrating asymptotic convergence of the adaptive SSRLS estimator.

Conflict of Interest :

There is no conflict of interest.

References

I. Aquilué-Llorens, David, and Aureli Soria-Frisch. "Eeg artifact detection and correction with deep autoencoders." *arXiv preprint arXiv:2502.08686* (2025). 10.48550/arXiv.2502.08686.

II. Arpaia, Pasquale, et al. "A Systematic Review of Techniques for Artifact Detection and Artifact Category Identification in Electroencephalography from Wearable Devices." *Sensors*, vol. 25, no. 18, 2025, p. 5770. 10.3390/s25185770

III. Beach, Christopher, Mingjie Li, Ertan Balaban, and Alexander J. Casson. "Motion Artifact Removal in Electroencephalography and Electrocardiography by Using Multichannel Inertial Measurement Units and Adaptive Filtering." *Healthcare Technology Letters*, vol. 8, no. 5, 2021, pp. 128–138. 10.1049/htl2.12016

IV. Behera, Sandhyalati, and Mihir Narayan Mohanty. "A Statistical Approach for Ocular Artifact Removal in Brain Signals." *2018 2nd International Conference on Data Science and Business Analytics (ICDSBA)*, IEEE, 2018, pp. 500–503. 10.1109/ICDSBA.2018.00099**.**

V. Behera, Sandhyalati, and Mihir Narayan Mohanty. "Artifact Removal Using Deep WVFLN for Brain Signal Diagnosis through IoMT." *Measurement: Sensors*, vol. 24, 2022, article 100465. 10.1016/j.measen.2022.100465.

VI. Behera, Sandhyalati, and Mihir Narayan Mohanty. "Removal of artifact from the brain signal using Discrete Cosine Transform." *International Conference on Emerging Trends and Advances in Electrical Engineering and Renewable Energy*. Singapore: Springer Nature Singapore, 2020. 10.1007/978-981-15-4992-2_23.

VII. Goldberger, Ary L., et al. "PhysioBank, PhysioToolkit, and PhysioNet: Components of a New Research Resource for Complex Physiologic Signals." *Circulation*, vol. 101, no. 23, 2000, pp. E215–E220. 10.1161/01.CIR.101.23.e215**.**

VIII. Judith, A. Mary, S. Baghavathi Priya, and Rakesh Kumar Mahendran. "Artifact Removal from EEG Signals Using Regenerative Multi-Dimensional Singular Value Decomposition and Independent Component Analysis." *Biomedical Signal Processing and Control*, vol. 74, 2022, article 103452**.** 10.1016/j.bspc.2021.103452.

IX. Klados, Manousos A., and Panagiotis D. Bamidis. "A Semi-Simulated EEG/EOG Dataset for the Comparison of EOG Artifact Rejection Techniques." *Data in Brief*, vol. 8, 2016, pp. 1004–1006. **10.1016/j.dib.2016.07.068.**

X. Lee, Young-Eun, No-Sang Kwak, and Seong-Whan Lee. "A real-time movement artifact removal method for ambulatory brain-computer interfaces." *IEEE Transactions on Neural Systems and Rehabilitation Engineering* 28.12 (2020): 2660-2670. 10.1109/TNSRE.2020.3032431.

XI. Liu, Chang, and Cheng Zhang. "Remove Artifacts from a Single-Channel EEG Based on VMD and SOBI." *Sensors*, vol. 22, no. 17, 2022, article 6698. 10.3390/s22176698

XII. Maddirala, Ajay Kumar, and Kalyana C. Veluvolu. "SSA with CWT and k-means for eye-blink artifact removal from single-channel EEG signals." *Sensors* 22.3 (2022): 931. 10.3390/s22030931.

XIII. Mannan, Malik Muhammad Naeem, Muhammad Ahmad Kamran, and Myung Yung Jeong. "Identification and removal of physiological artifacts from electroencephalogram signals: A review." *IEEE Access* 6 (2018): 30630-30652. 10.1109/ACCESS.2018.2842082

XIV. Massar, Hicham, Tarik Ben Drissi, Badr Nsiri, and Mohamed Miyara. "Advancements in Blind Source Separation for EEG Artifact Removal: A Comparative Analysis of Variational Mode Decomposition and Discrete Wavelet Transform Approaches." *Applied Acoustics*, vol. 228, 2025, article 110300. 10.1016/j.apacoust.2024.110300.

XV. Mumtaz, Wajid, Suleman Rasheed, and Alina Irfan. "Review of challenges associated with the EEG artifact removal methods." *Biomedical Signal Processing and Control* 68 (2021): 102741. 10.1016/j.bspc.2021.102741

XVI. Panda, Sreelekha, et al. "Epileptic seizure detection using deep ensemble network with empirical wavelet transform." *Measurement Science Review* 21.4 (2021): 110-116. 10.2478/msr-2021-0016.

XVII. Pei, Yan, et al. "DTP-Net: Learning to reconstruct EEG signals in time-frequency domain by multi-scale feature reuse." *IEEE Journal of Biomedical and Health Informatics* 28.5 (2024): 2662-2673. 10.1109/JBHI.2024.3358917.

XVIII. Raj, Vandana Akshath, Tejasvi Parupudi, Vishnumurthy Kedlaya K, Ananthakrishna Thalengala, and Subramanya G. Nayak. "Physiological Artifact Suppression in EEG Signals Using an Efficient Multi-Scale Depth-Wise Separable Convolution and Variational Attention Deep Learning Model for Improved Neurological Health Signal Quality." *Technologies*, vol. 13, no. 12, 2025, article 578. 10.3390/technologies13120578.

XIX. Ranjan, Rakesh, Bikash Chandra Sahana, and Ashish Kumar Bhandari. "Motion artifacts suppression from EEG signals using an adaptive signal denoising method." *IEEE Transactions on Instrumentation and Measurement* 71 (2022): 1-10. 10.1109/TIM.2022.3163062.

XX. Sayed, Ali H., and Thomas Kailath. "A State-Space Approach to Adaptive RLS Filtering." *IEEE Signal Processing Magazine*, vol. 11, no. 3, 1994, pp. 18–60. 10.1109/79.295229

XXI. Xing, Le, and Alexander J. Casson. "Deep Autoencoder for Real-Time Single-Channel EEG Cleaning and Its Smartphone Implementation Using TensorFlow Lite with Hardware/Software Acceleration." *IEEE Transactions on Biomedical Engineering*, vol. 71, no. 11, 2024, pp. 3111–3122. 10.1109/TBME.2024.3408331.